On the relevance of kinking to reversible hysteresis in MAX phases

N.G. Jones [a], C. Humphrey [a], L.D. Connor [b], O. Wilhelmsson [c], L. Hultman [d], H.J. Stone [a], F. Giuliani [e], W.J. Clegg [a,*]

[a] *Department of Materials Science & Metallurgy, 27 Charles Babbage Rd, Cambridge CB3 0FS, UK*
[b] *Diamond Light Source, Harwell Science & Innovation Campus, Didcot OX11 0DE, UK*
[c] *Sandvik Heating Technology AB, SE-734 27 Hallstahammar, Sweden*
[d] *Thin Film Physics Division, Department of Physics, Chemistry and Biology (IFM), Linköping University, SE-581 83 Linköping, Sweden*
[e] *Department of Materials, Imperial College, London SW7 2AZ, UK*

Abstract

This paper examines the idea that reversible hysteresis in MAX phases is caused by the formation, growth and collapse of unstable, or incipient, kink bands. In situ X-ray diffraction of polycrystalline Ti_3SiC_2 in compression showed that residual elastic lattice strains developed during the first loading cycle and remained approximately constant afterwards. These residual strains were compressive in grains with a low Schmid factor and tensile in grains with a high Schmid factor, consistent with previous observations of plastically deformed hexagonal metals. In contrast, incipient kink bands would be expected to collapse completely, without any residual strain. Elastoplastic self-consistent simulations showed that reversible hysteresis is predicted if some grains yield by slip on the basal plane, while others remain predominantly elastic, giving both the experimentally observed magnitude of the work dissipated and its dependence on the maximum applied stress. The reversible hysteresis in single crystals was studied by cyclically indenting thin films of Ti_3SiC_2 and Ti_3SiC_2/TiC multilayers on Al_2O_3 substrates. The work dissipated in the multilayer films was greater than in Ti_3SiC_2 alone, despite the reduction in volume fraction of Ti_3SiC_2. Reversible hysteresis was also observed during indentation of single-crystal cubic MgO, demonstrating that this behaviour can occur if there are insufficient slip systems to accommodate the strain around the indentation. These results show that reversible hysteresis is associated with conventional dislocation flow, without the need for unstable kinking.

© 2014 The Authors. Published by Elsevier Ltd. on behalf of Acta Materialia Inc. Open access under CC BY license.

1. Introduction

A group of ternary, layered carbides and nitrides, known as MAX phases, show a large reversible hysteresis when they are repeatedly loaded and unloaded. This effect is seen in a wide range of materials, both in polycrystals under compression [1–4] and in single crystals during indentation [5–11]. The hysteretic behaviour has been divided into two types: Type I, where all cycles are completely reversible, as in Ti_3SiC_2; and Type II, where the first loading cycle causes some permanent strain, as in graphite, after which the behaviour is completely reversible [3]. Both have generally been associated with crystals that have anisotropic, often hexagonal structures, with a c/a ratio typically >1.5 [3].

It is well known that in soft hexagonal metals, such as Cd or Zn [12,13], dislocations move much more easily on the basal planes than on the prismatic or pyramidal planes. However, if the soft slip planes are oriented so that they are parallel to the loading axis, deformation can occur by kinking, where two dislocation walls are nucleated by the

* Corresponding author.
  E-mail address: wjc1000@cam.ac.uk (W.J. Clegg).

sequential breaking of individual crystal planes [14]. Each wall contains dislocations gliding on the basal plane with the same Burgers vector, but of opposite line vector to the opposing wall. Inspired by these ideas, Barsoum and co-workers [15,16] have suggested that deformation in MAX phases can also take place by kinking and it is often stated that the linear features observed in deformed structures are the walls of kinks [17,18].

The driving force for the formation of a kink comes from the extra work done by the applied force and the changes in elastic energy in the body. It is resisted by the attractive forces between the dislocations formed by breaking of the crystal planes. In a manner similar to a crack under tension, a kink must reach a minimum length before it becomes stable [14]. Therefore, in any deforming material, there may be kink bands shorter than this critical value, so that when the material is unloaded these subcritical kinks, termed incipient kink bands, will disappear completely. It is thought that the formation, growth and subsequent collapse of these small kinks gives rise to the reversible strain on cyclic loading [1]. In a polycrystal, kinking is thought to occur in those grains whose basal planes are approximately parallel to the loading axis. However, grains with slip planes on which the resolved shear stresses are higher will deform by dislocation motion [1]. In both cases, agreement has been obtained between observations and an analysis based on these ideas, in particular that the work dissipated in a reversible cycle is proportional to the square of the maximum applied stress [3].

In indentation, the work dissipated has been observed to vary with the maximum stress, in the same manner as in the uniaxial compression tests [1,3]. Generally, where the number of slip systems was restricted, e.g. basal slip only in Ti_3SiC_2, changes of orientation had little effect [5]. However, if changing the orientation caused the number of operative slip systems to increase, the work done in a reversible hysteresis loop decreased [9].

In the process of kinking, it is considered that the work dissipated is associated with the plastic work done during both the growth and subsequent collapse of the kink, while the reversibility of flow is associated with the attractive forces between the dislocations in the kink band wall, with a smaller contribution from the relaxation of dislocation pile-ups. However, as the incipient kink band collapses, the attractive forces between the opposing walls increase, such that the band will be able to collapse completely [1,10,11], provided effects such as dislocation entanglement are minimal. Easy flow, with no cross-slip and dislocation interaction, has indeed been observed in these materials [19], so that any residual strains in the sample once it had been unloaded would be negligible. Other sources of elastic strains, such as the generation of long-range lattice strains [20–24], are also considered to be negligible [3]. However, to date, no direct evidence has been obtained for unstable, or incipient, kink bands.

Experimental studies of both polycrystalline and single-crystal Ti_3SiC_2 have been carried out, seeking to examine the idea that this reversible hysteresis is associated with kinking. By using in situ synchrotron X-ray diffraction during compression testing, direct measurements can be obtained of the volume averaged elastic strains that develop in a polycrystalline MAX phase as it is cyclically deformed, and in particular, the sign and magnitude of the elastic strains in grains of different orientations. Additional data on the cyclic deformation behaviour of Ti_3SiC_2 has been obtained by comparing the cyclic indentation behaviour of single-crystal thin films of Ti_3SiC_2 and multilayers of TiC/Ti_3SiC_2, to investigate the effect of reducing the volume fraction of Ti_3SiC_2. The extent to which reversible hysteresis can be obtained in other materials has also been studied through measurements of the well-characterized cubic material, MgO.

2. Experimental

2.1. Materials

2.1.1. Polycrystals

Cylindrical, polycrystalline specimens were made by electrical discharge machining of a commercially produced, hot-pressed bar of Ti_3SiC_2 (3-ONE-2, Voorhees, NJ, USA). The samples for ex situ cyclic compression testing had a diameter of 6 mm and length of 15 mm, whilst those for in situ diffraction experiments had a diameter of 3 mm and a gauge length of 7 mm. The material had a non-random texture and a somewhat bimodal grain structure, with some large grains, ~25 μm, in a matrix of grains with a mean size of 8 μm.

2.1.2. Single crystals

TiC (0 0 1) and Ti_3SiC_2 (0 0 0 1) single-crystal films, as well as TiC (1 1 1)/Ti_3SiC_2 (0 0 0 1) multilayers, were grown on Al_2O_3 (0 0 0 1) substrates by unbalanced magnetron sputtering under ultrahigh-vacuum conditions, as described in Ref. [25]. The TiC/Ti_3SiC_2 had layers of equal thickness, each of 10 nm. The single crystal of MgO (MTI Crystal, Richmond, CA, USA) had an (0 0 1) orientation.

2.2. Ex situ testing

Initial ex situ tests were carried out to confirm that the polycrystalline material showed reversible hysteresis. Samples were cycled five times from zero to a peak stress of 400 MPa under load control at an equivalent strain rate of $5 \times 10^{-6} \text{ s}^{-1}$ with the strain in the axial direction being measured using a strain gauge (Kyowa, Japan) attached directly to the sample surface.

2.3. In situ X-ray diffraction

In situ loading of the polycrystalline Ti_3SiC_2 was conducted on the I12 beamline at the Diamond Light Source. The beamline was configured in Debye–Scherrer transmission geometry, and a monochromatic incident beam of

500 μm × 500 μm with an energy of 82.2 keV ($\lambda = 0.1508$ Å) was used. Diffraction images were gathered throughout the loading cycles using a Pixium area detector. A schematic representation of the experimental configuration is shown in Fig. 1a.

The samples were subjected to five compressive loading cycles, between zero and a peak stress of 460 MPa using an electrothermal mechanical tester. Each cycle was conducted under load control at an equivalent strain rate of $5 \times 10^{-6} \, \text{s}^{-1}$. Diffraction images had an exposure time of 0.4 s, and were acquired at a frequency of 0.25 Hz, thereby giving a strain resolution of 2×10^{-5}. The evolution of strain on individual lattice planes was evaluated using the diffraction data acquired from two 10° segments, centred about the compression axis (azimuthal angles of 0° and 180°), as shown in Fig. 1b. Azimuthal sectioning and radial integration was performed using Fit2D [26], and individual peak fitting conducted using a Gaussian function in Wavemetrics Igor Pro. The lattice strain, ε_{hkl}, from grains with *hkl* planes fulfilling diffraction criteria was calculated from the change in interplanar spacing, d_{hkl}, relative to the initial spacing, d_{hkl}^i, as described in Ref. [27].

The bounds and average values of the Schmid factor associated with the grains corresponding to each Bragg reflection, *hkl*, were calculated taking into account the diffraction angle and the range of azimuthal angles used to collect the data.

2.4. Cyclic indentation

Cyclic indentation on the single-crystal thin-film samples and an MgO crystal was carried out using a nanoindenter (Hysitron Triboscope) with a Berkovich tip. Samples were loaded up to a maximum load of 6 mN and then unloaded to 0.6 mN in 5 s. This cycle was repeated a further three times before completely unloading. No cracking was observed around any of the indentations. For comparison, the MgO crystal was also indented to a load of 50 mN using a Berkovich tip in a nanoindenter (Micromaterials, Nanotest) to see whether stable kinks formed in the plastic zone.

The indents were cross-sectioned using a focused ion beam workstation (Zeiss, Cross-beam 1540 ESB) to make electron-transparent foils that could be viewed in a transmission electron microscope (FEI, Tecnai) operating at 200 kV.

2.5. EPSC modelling

To simulate the macroscopic stress–strain behaviour, elastoplastic self-consistent (EPSC) modelling was used [20,21]. This approach is derived from Eshelby's homogeneous inclusion method [28,29], in which each grain is treated as embedded in a homogeneous medium that has the properties of the aggregate, but where each grain has the single-crystal elastic and plastic properties of Ti_3SiC_2. Using this approach, it is possible to estimate the macroscopic behaviour of the material.

3. Results and discussion

3.1. Polycrystals in compression

3.1.1. Development of residual lattice strains

Fig. 2 shows a stress–strain curve obtained when polycrystalline Ti_3SiC_2 was cycled ex situ five times to a peak stress of 400 MPa. The sample deformed elastically with a measured Young's modulus of 324 GPa, after which yielding occurred at ∼80 MPa in the first cycle, suggesting a shear yield stress of 40 MPa. On unloading, there was a small residual strain. Subsequent cycles showed the fully reversible behaviour described by Barsoum and co-workers [1,3], with a dissipated energy of 0.037 MJ m^{-3}. However, unlike the observations of Barsoum and co-workers [1,15], there was always a small residual plastic strain on the first cycle. Fully reversible behaviour was only observed for subsequent cycles.

The in situ X-ray experiments showed that these residual lattice strains developed in the first cycle and remained approximately constant with further cycling (Fig. 3). The measured residual strains varied both in magnitude and sign between the different families of grains, with the
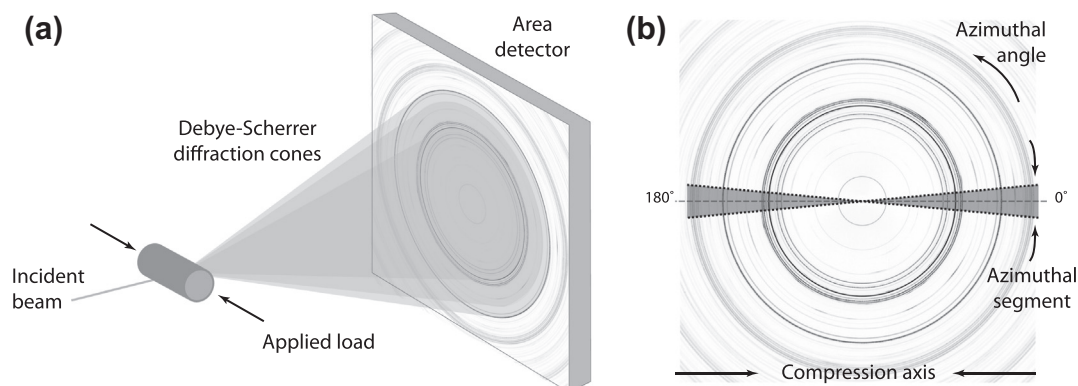

Fig. 1. (a) Schematic illustration of the beamline configuration used for in situ synchrotron X-ray diffraction, adapted from Fig. 2a in Ref. [43], and (b) the azimuthal segments from which the diffraction data was taken.
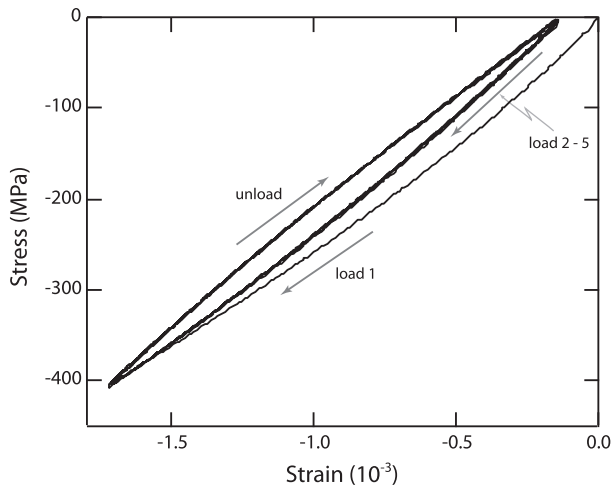
Fig. 2. Stress–strain curve for Ti$_3$SiC$_2$ loaded and then unloaded five times in compression to 400 MPa.

Fig. 4. The influence of Schmid factor on the measured value of the lattice strain, using the diffraction data from the 0° segment. Similar trends were seen in the 180° segment.

maximum residual strain, in (0 0 *l*)-type grains being compressive and ~1.3 times the yield strain, estimated from the macroscopic yield stress and Young's modulus. As described in the Introduction, fully recoverable incipient kink bands would result in negligible residual lattice strains. Therefore, the measurement of these residual strains is inconsistent with the idea that hysteresis is associated predominantly with incipient kink bands.

Fig. 4 shows that the grains that have their basal planes oriented at either very high, e.g. (0 0 6), or very low, e.g. (2 0 0), angles to the compression axis, i.e. with low Schmid factors, were associated with compressive, residual lattice strains. Those grains that have their basal planes at some intermediate angle, e.g. (1 0 7) or (1 0 9), to the compression
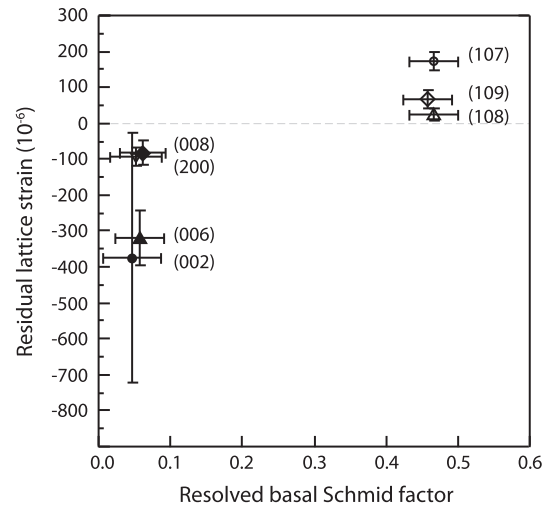
axis, i.e. with high Schmid factors, were associated with tensile, residual lattice strains. This is consistent with measurements of residual elastic lattice strains in other polycrystalline materials that have deformed plastically in compression [21,30].

The development of elastic lattice strains can be understood qualitatively using a two-bar model, which has also been used to explain Bauschinger effects in two-phase alloys [31]. Here, one bar represents the soft, plastically deforming grains and the other the hard, elastic grains. In this case, the former is associated with those grains favourably oriented for slip and the latter with those unfavourably oriented for slip. It is assumed the volume
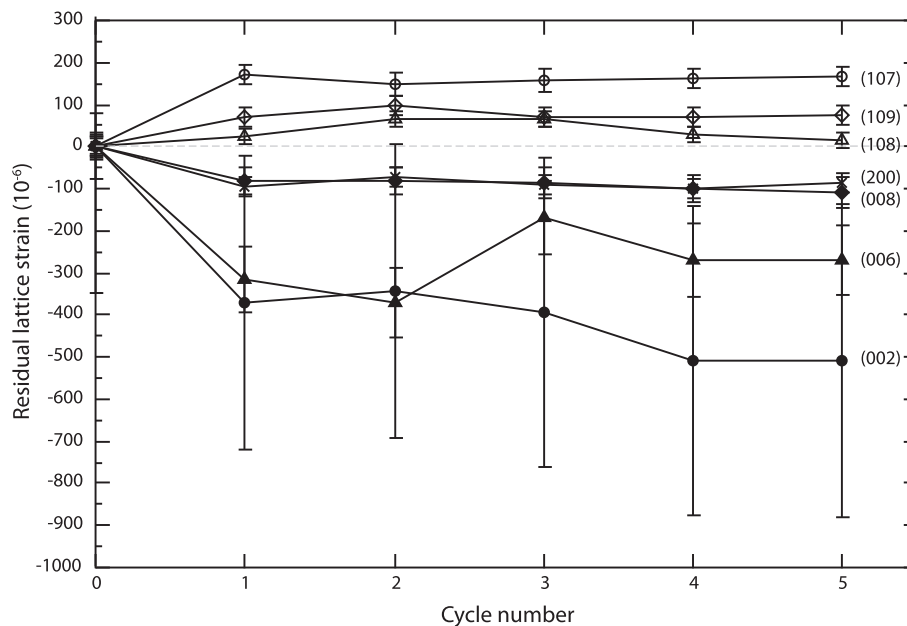

Fig. 3. The residual or zero stress lattice strains vs. cycle number for different reflections, using the diffraction data from the 0° segment. Similar trends were seen in the 180° segment.

fraction of each type of grain is equal. If an increasing compressive stress is applied, both bars will deform elastically at first. However, at stresses above the yield point of the soft bar, the elastic strains in the bar will remain approximately constant, increasing only in line with strain hardening. The increasing load must therefore be borne by the hard bar, so that the elastic strain increases more rapidly than at first [32]. On unloading, plastic flow ceases and the compressive stresses in both bars decrease in magnitude at a rate given by their respective elastic moduli. However, if the yield strength of the soft bar is sufficiently low, then the stress in the soft bar will reach its tensile yield strength before the hard bar has fully unloaded. On further unloading of the system, the soft bar will continue to plastically deform in tension until the applied load decreases to zero. On loading, the soft bar underwent an elastic strain equal to $-\varepsilon_Y$, but on unloading there was a tensile strain of $2\varepsilon_Y$. This gives rise to the residual elastic strain, which, in this case, must have a magnitude approximately equal to the yield strain, as shown in Fig. 2.

At the end of the first cycle, the soft bar is plastically deforming in tension, so that on reloading in compression, yield will not start until the stress in the soft bar reaches its compressive yield stress. This occurs after an elastic strain of magnitude $-2\varepsilon_Y$, at an applied tensile stress of $2\sigma_Y$, or, in terms of the critical resolved shear stress on the basal plane, $4\tau_Y$. On unloading, the sample will once again undergo an elastic strain of $2\varepsilon_Y$, before tensile yielding starts in the soft grains, with further elastic loading borne by the hard grains. Once the sample has been completely unloaded the stress in the soft grains will be equal to their tensile yield stress, while the hard grains will be at a balancing stress in compression.

The first cycle is required to set up the internal stress-state needed for reversible hysteresis to occur. This is entirely consistent with the observation that the elastic strains change reversibly after the first loading cycle. It also suggests that Type II behaviour should always be observed. However, it might be imagined that if the sample were deformed prior to testing, perhaps during hot-pressing, the initial stage would not be observed.

Calculations of the elastic constants suggest that the material has a maximum anisotropy of only 15% [33], so that if variations in orientation alone account for the fact that some grains plastically deform whilst others do not, there must be a high degree of plastic anisotropy. This appears to be the case in Ti_3SiC_2, where basal slip has been reported to occur at shear stresses as low as 36 MPa [16]. Flow on other slip systems in Ti_3SiC_2 under compression has not been reported. This is also consistent with hardness measurements in Ti_3SiC_2, which are $\sim$18–24 GPa [34] for Ti_3SiC_2 thin films oriented with the basal plane perpendicular the indenter, although lower values have been reported when cracking occurs [35–37]. As the hardness is determined primarily by the flow stress of the harder slip system [38,39], this would suggest that the shear flow stress on the other slip systems is greater than $\sim$3–4 GPa. However, as

delamination is often observed [17], this may be a lower bound.

3.1.2. Numerical simulations of plastic flow in polycrystalline Ti_3SiC_2

Although the two-bar model can be a useful qualitative tool, it cannot be used to make quantitative estimates of the macroscopic behaviour of a polycrystalline aggregate. Numerical simulations were therefore conducted using EPSC modelling [20,40].

These simulations require information on the single-crystal elastic constants and on the yield and hardening behaviour. As there are no measurements of the single-crystal elastic constants, the results of the simulations by Yu et al. [33] have been used, where $c_{11} = 360$ GPa, $c_{12} = 84$ GPa, $c_{13} = 101$ GPa, $c_{33} = 350$ GPa, $c_{44} = 158$ GPa. This gives a value for the Young's modulus along the c-axis of 300 GPa, and along the a-axis of 325 GPa, with a maximum value of 355 GPa. In the EPSC model constructed, the plastic flow behaviour was characterized simply by a shear yield stress. The yield stress on other slip systems was set at 2 GPa, which was sufficiently high to ensure flow does not occur. For simplicity, and because there was insufficient information to select suitable values, we have neglected the work-hardening behaviour. Therefore, the simulations can only be considered as approximate.

Using a maximum applied stress of 460 MPa, and with yielding only on the basal plane at a shear yield stress of 50 MPa, the EPSC modelling predicts that after an initial loading and unloading there should be a residual strain, as observed, after which reversible hysteresis occurs (Fig. 5). In other words, the hysteretic effect could be explained by the generally accepted ideas that describe the deformation of polycrystalline aggregates [20,41]. The EPSC calculations also showed that, for the hysteresis to be observed, the sample must be loaded to some minimum
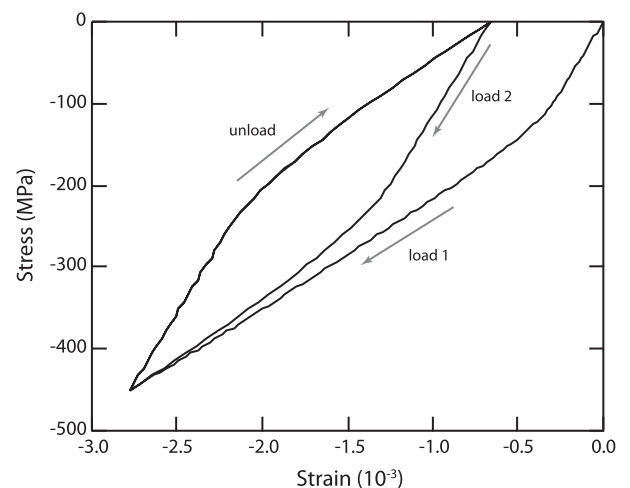

Fig. 5. Stress–strain curve predicted using EPSC simulation, with a shear yield stress of 50 MPa on the basal plane, a yield stress on other slip systems of 2 GPa and the elastic data of Yu et al. [33].

stress whose magnitude was approximately twice the applied compressive yield stress, or four times the minimum shear yield stress.

One of the most compelling predictions of the incipient kink band model was that the work dissipated, W_d, in the reversible cycles varied with the maximum applied stress, σ, approximately as:

$$W_d \propto \sigma^2.$$

The power of 2 was approximately consistent with the experimental observations, within any experimental error, with values of ~2.2 for a coarse-grained (42 μm) material and ~2.5 for a fine-grained (8 μm) material [3].

The work dissipated during reversible hysteresis, W_d, was estimated using the EPSC method and, because of the apparent differences in yield stress, the calculations were repeated for values of the uniaxial yield stress ranging from 10 to 75 MPa. The results are shown in Fig. 6, which shows that the EPSC simulations can give reasonable agreement with the experimentally observed values of W_d and correctly predict the general variation of W_d with respect to σ. This is particularly impressive as the EPSC model contains only the elastic constants and the yield stresses as variables.

The value of the observed exponent, n, in the relationship $W_d \propto \sigma^n$ depends on the range of stresses over which this is measured. If the measurements are made at maximum applied stresses much greater than the yield stress on the basal slip system, the value of n is approximately unity (Fig. 6). However, measurements are generally made over the full range of stress where hysteresis is observed and much higher values can be observed, particularly if one were only to measure at stresses close to the yield stress. This results in the exponent increasing as one approaches the critical stress below which reversible hyster-

esis is not observed. The resulting curvature can be clearly seen in the data plotted in Fig. 6.

The energy dissipated also varies with the grain size. The onset of hysteretic behaviour has been observed at compressive stresses of ~50 and ~105 MPa for coarse- and fine-grained materials [3], suggesting shear yield stresses of ~25 and ~52 MPa, respectively. A decrease in the grain size by a factor of 5 (from 42 to 8 μm) has therefore increased the yield strength by approximately a factor of 2, close to what would be expected from the conventional Hall–Petch relationship.

This suggests that the grain boundaries were acting as the predominant obstacles to dislocation motion, which is consistent with the observed temperature independence of flow on the basal slip system [42]. It is therefore tentatively suggested that the increase in W_d with decreasing grain size occurs due to changes in the yield stress associated with changes in the grain size. That grain boundaries can act as the predominant obstacle to flow only occurs because slip on the basal plane occurs at such low stresses.

3.1.3. Development of elastic lattice strains during the first loading cycle

To investigate the idea that in polycrystalline Ti₃SiC₂ some grains are deforming elastically, while others are plastically deforming, X-ray experiments were carried out to study the behaviour of different groups of grains during loading and unloading. Since slip in Ti₃SiC₂ is thought to occur only on the basal plane, four subsets of grains were studied, where the basal planes in each subset were aligned at a different angle to the loading direction. These were the (2 0 0)- and (0 0 6)-type grains, which were at 3° and 88.7°, respectively, to the compression axis, and the (1 0 7) and (1 0 9) reflections, where the basal planes were at 44° and 37° to the loading direction, respectively.

The evolution of the elastic lattice strains measured from the (2 0 0), (0 0 6), (1 0 7) and (1 0 9) reflections during the first loading and unloading cycle are shown in Fig. 7. Conventional polycrystalline plasticity theory predicts that, at first, all grains load elastically, until a stress is reached at which the softest grains yield. Beyond this stress, the soft grains cannot support any increase in the lattice strain, so that the increasing applied load must be borne by the harder grains, so that their elastic lattice strains must increase more rapidly than before [22]. Such load carrying is seen in the (0 0 6) grains in both the 0° and 180° segments, and the (2 0 0) in the 180° segment, the latter of which is a particularly good example of this type of behaviour. Here, the lattice strain first increased linearly with the applied stress, to ~300 MPa, after which the rate of lattice strain accumulation increased, indicating these grains were carrying load. When the applied stress was removed these grains unloaded elastically, producing a net compressive residual elastic lattice strain, as shown in Fig. 3. The lattice strains from the (0 0 6) grains across the two compressive azimuthal segments show similar behaviour, although the data had increased point-to-point scatter as a result of
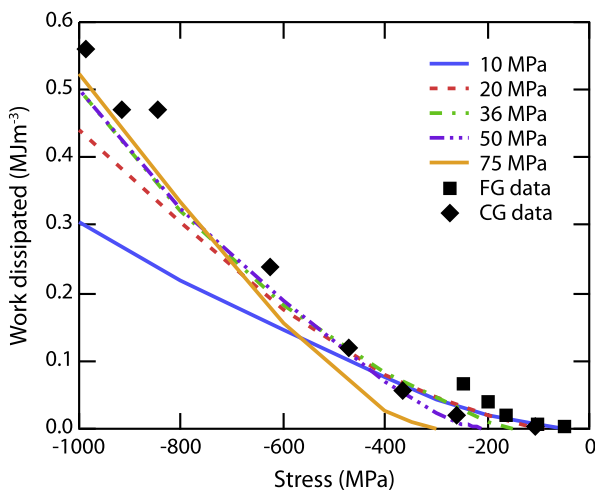

Fig. 6. EPSC predictions of work dissipated during cyclic loading for Ti₃SiC₂ with various shear yield stresses, compared with experimental data with 8 μm (fine-grained), and 42 μm (coarse-grained) grain sizes (data from Ref. [3]).
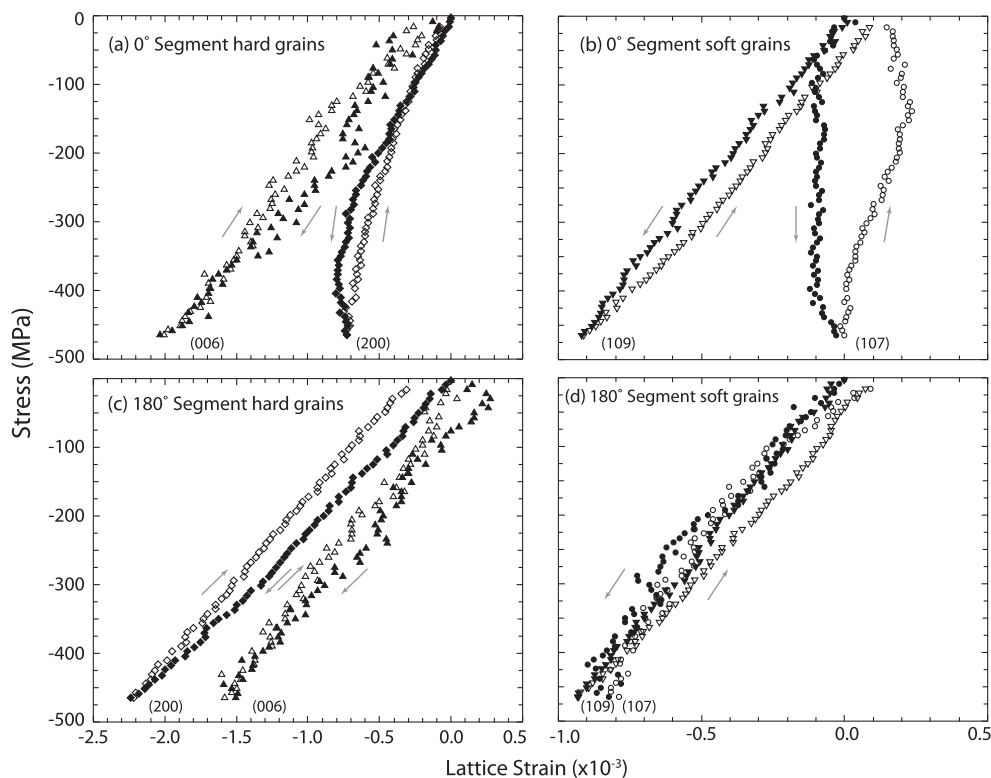
Fig. 7. Graphs of lattice strain vs. stress during the first loading and unloading cycle for (a) the (006) and (200) and (b) the (109) and (107) reflections from the 0° segment on the Debye–Scherrer rings, and (c) the (006) and (200) and (d) the (109) and (107) reflections from the 180° segment. Closed symbols = loading, open symbols = unloading. For clarity, error bars are not plotted, but have a similar magnitude to those shown in Fig. 3 for the relevant peak.

the inferior counting statistics from these weaker peaks. The behaviour of the (200) in the 0° segment is more akin to what would be expected of a plastically deforming grain, as the rate of lattice strain accumulation decreased with greater applied loads. This observation, and the discrepancy between the two segments was surprising, and will be discussed later.

The lattice strain evolution during loading of the soft (109) grains was linear up to a stress of ~70 MPa. At higher stresses, the rate of lattice strain accumulation with applied stress decreased, indicative of grains which have yielded. However, despite the fact they were yielding, the elastic lattice strains increased. On unloading to a stress between 200 and 150 MPa, the elastic lattice strain varied with applied stress at a rate similar to that of the initial loading, suggesting that deformation was elastic. Below 150 MPa, the grains continued to unload but the rate of change of lattice strain with applied stress decreased. The behaviour was nearly identical between the two azimuthal segments and resulted in the net tensile residual elastic lattice strain shown in Fig. 3.

Idealized elastic–plastic behaviour, typical of face-centred or body-centred cubic metals, predicts that on loading the elastic lattice strain accumulates until the grain yields, after which there are no further changes in elastic lattice strain beyond that associated with work hardening. However, for this to occur, the grain must be able to undergo any shape change, i.e. it must have five independent

slip systems. For a material where slip is only possible on the basal plane, such as Ti_3SiC_2, there are only two independent slip systems, so that any plastic flow must be accommodated by elastic strain. Therefore, in such systems, as here, one would expect the elastic lattice strains to continue increasing in soft grains above their yield stress. Similar behaviour has been observed within the bulk of a carburized stainless steel [24].

Interpretation of the lattice strain evolution in the (107) grains, Fig. 7, is more complex, as there are significant differences between the behaviour in the two azimuthal segments. During loading, the grains in the 0° segment deform elastically up to ~70 MPa, after which ideal flow occurred, with no further lattice strain accumulation. At a stress of 400 MPa, the lattice strain decreased to zero. This relaxation is consistent with permanent damage in the crystal, such as the formation of a crack or a delamination of planes [15,16]. On unloading, the grains initially unload to ~375 MPa without any change in lattice strain, possibly associated with the damage suggested to have occurred during the later stages of loading, and could, for example, correspond to the straightening of delaminated sections. As the compressive stress decreased from 375 to 150 MPa, the rate at which elastic lattice strain decreased with applied stress at a rate similar to that on initial loading. At a stress <150 MPa, the rate of change of lattice strain decreased, suggesting the onset of plastic flow, driven by the unloading of the hard grains. In contrast, the

lattice strain evolution in the grains from the 180° segment was similar to that of the (109) planes.

Whilst the measured lattice strains in the (109) and (006) grains showed analogous behaviour in both the 180° and 0° segments, significant differences were observed between the responses of the (107) and (200) grains in these segments. The measured lattice strains suggest that the (107) and (200) orientated grains in the 0° segment deform more easily than those in the 180° segment (Fig. 7). This apparent asymmetry in deformation response around the compression axis could be associated with slight misalignment or geometric imperfections of the sample during compression testing. However, if this were the case, a similar effect should be observed in both the (107) and (109) grains. An alternative possibility is the presence of large grains within the diffraction gauge volume and non-random textures. In such cases, the lattice strain response may be biased by the response of the large grains. Indeed, there is evidence for this, as significant variations in the intensity of the (107) and (200) reflections were observed around the Debye–Scherrer rings. In addition, differences in the local constraint imposed by surrounding grains will also affect the measured lattice strain. This latter effect has been observed previously in the deformation of a binary nickel–titanium shape memory alloy [43].

Critically, in spite of the differences between the 180° and 0° segments, the grains in soft orientations to the loading axis all accumulate tensile residual lattice strains whilst those in the hard orientations exhibit compressive residual lattice strains. These observations are again consistent with conventional plasticity theory of polycrystals.

Fig. 8 shows the changes in the fitted peak areas during the first loading/unloading cycle. Again, the data from the 0° segment (Fig. 8a) shows a more pronounced effect than the 180° segment (Fig. 8b). For the former, there was a continuous 4-fold decrease in the fitted area of the (200) diffraction peak, indicating that the volume of associated diffracting material was changing by this amount. At the same time, there was an increase in the fitted area of the

(107) diffraction peak, suggesting that in the first loading cycle those basal planes at the lowest angles, i.e. approximately parallel to the loading axis, are tending to reorient to higher angles. Importantly, the areas of the peaks were not fully recovered during the unloading cycles, suggesting residual reorientations of material as a result of the first loading cycle. A similar effect can be seen in the data from the 180° peaks (Fig. 8a), although the changes were much smaller. In both cases, the fitted area of the (006) and the (109) diffraction peaks remain constant.

3.1.4. Change of elastic lattice strains during the second loading cycle

The elastic lattice strains measured from the (200), (006), (107) and (109) reflections during the second loading cycle are shown in Fig. 9. The lattice strain evolution on reloading follows the same path as that of unloading in the first cycle. For those grains that had deformed plastically in the first loading/unloading cycle, closed hysteretic loops are observed, suggesting reversible plastic responses from these grains. The notable exception are the (107) grains in the 0° segment, which follow the same path as the unloading of cycle 1 during all subsequent loading/unloading cycles. This may be attributed to the permanent nature of any delamination damage that occurred during the first loading cycle, as suggested above, and the subsequent deformation of these damaged regions by plastic bending and straightening. For any given reflection, significant differences in lattice strain, at a given applied stress, are only observed in the loading segment of the first cycle. This is consistent with establishing balanced intergranular lattice strains via plastic deformation in the first loading cycle. Similar trends can be seen in the fitted peak areas (Fig. 10), which indicates that the large changes in diffracting volume are almost completely recovered, consistent with the macroscopically observed reversible hysteresis.

In summary, the data presented here suggests that the hysteresis effect observed in polycrystalline MAX phases is broadly consistent with conventional descriptions of
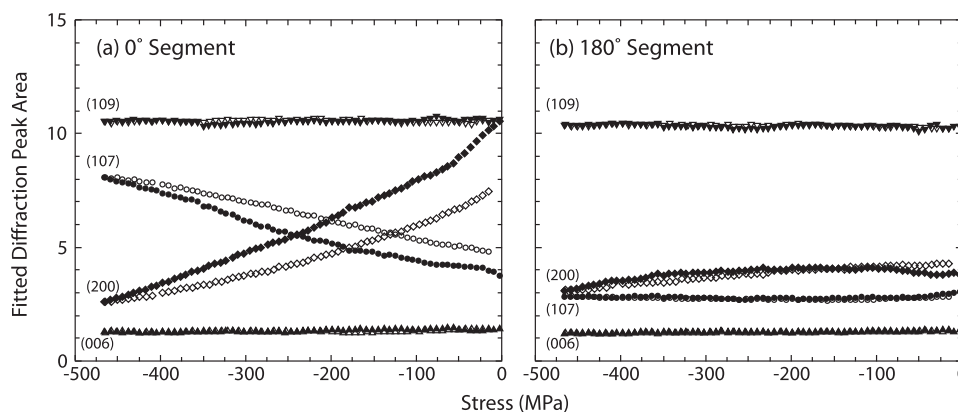

Fig. 8. Evolution of the fitted peak area changes with stress during the first loading cycle for the (006), (200), (109) and (107) diffraction peaks, taken from (a) the 0° and (b) the 180° segments on the Debye–Scherrer rings. Closed symbols = loading, open symbols = unloading. For clarity, error bars are not plotted, but are approximately the size of the data points.
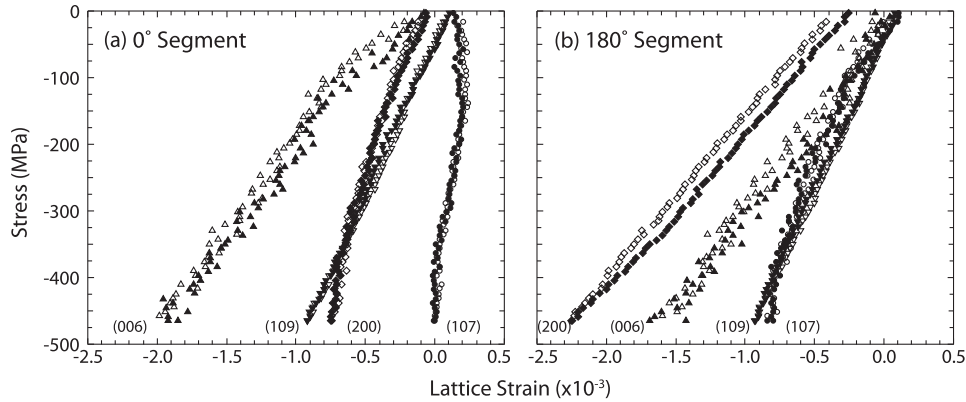
Fig. 9. Graphs of lattice strain vs. stress during the second loading and unloading cycle for the (006), (200), (109) and (107) reflections taken from (a) the 0° and (b) the 180° segments on the Debye–Scherrer rings. Closed symbols = loading, open symbols = unloading. For clarity, error bars are not plotted, but have a similar magnitude to those shown in Fig. 3 for the relevant peak.
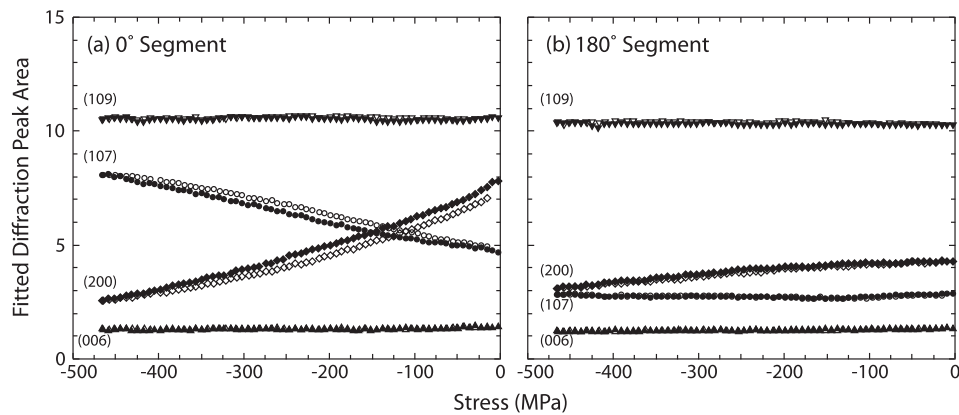

Fig. 10. Evolution of the fitted peak area changes with stress during the second loading cycle for the (006), (200), (109) and (107) diffraction peaks, taken from (a) the 0° and (b) the 180° segments on the Debye–Scherrer rings. Closed symbols = loading, open symbols = unloading. For clarity, error bars are not plotted, but are approximately the size of the data points.

plastic polycrystals, where the basal slip systems are very soft. During loading, elastic strains build up in the hard grains, which are sufficient to drive reverse flow in the soft grains on unloading, thereby giving rise to hysteresis. The constraint imposed on soft grains by surrounding hard grains and the limited number of available slip systems will also contribute to the development of elastic lattice strains. These ideas are consistent with the observed development of residual elastic lattice strains, compressive in hard grains and tensile in soft grains, and with the correct prediction of both the magnitude of the hysteresis effect and its dependence on the applied stress using existing models for the plasticity of polycrystalline materials. It also shows why the effect appears to be associated with the yield stress, avoiding the need to find reasons why kinking occurs at stresses lower than predicted [3]. Furthermore, such a mechanism is consistent with the behaviour previously observed in other plastically anisotropic, polycrystalline materials. However, it is also clear that there are other phenomena superimposed on this basic framework, such as load shedding, possibly due to delamination, and differences

between the 0° and 180° segments that might be associated with microstructural variation.

3.2. Single crystals in nanoindentation

The mechanism above does not explain why reversible hysteresis is also seen when single crystals are indented. Experiments [38,39] and calculations [44] have shown that in indentation, as in a polycrystal, a sufficient number of independent slip systems must operate to give the strain required. In Ti_3SiC_2, dislocation motion has been seen to occur only on the basal plane. This gives insufficient slip systems to accommodate the indenter by plastic flow, causing a build up of elastic strains. If the sample were unloaded, relaxation of these elastic strains could give rise to reverse plastic flow and hence reversible hysteresis. This is similar to the two-bar model described earlier.

The idea that reversible hysteresis in single crystals is associated with accommodating the strain around the indenter in a material with either insufficient or very different types of slip system is also consistent with previous

observations. It is seen that the magnitude of the work dissipated is largely unaffected where there are only a limited number of slip systems [11,45,46], but decreases if the crystal orientation changes so that multiple slip systems can operate [8,9].

3.2.1. Importance of kinking in indentation

Kink-like features have often been observed in indented crystals [17,18,47], giving support to the idea that hysteresis is caused by the nucleation growth and collapse of subcritical kinks. To investigate whether this is the case, or whether hysteresis might be driven by internal stresses, the hysteresis of thin films of single-crystal thin films of Ti_3SiC_2 was compared with multilayer films in which some of the Ti_3SiC_2 had been replaced by TiC. Homogeneous TiC did not show reversible hysteresis (Fig. 11), and also has a higher flow stress [48] than Ti_3SiC_2. TiC is therefore likely to be an elastic element in the two-bar model. Removing kinking material, particularly as the TiC is also stiffer than the Ti_3SiC_2, would be expected to decrease the work dissipated during hysteresis, if this were associated with kinking.

In fact, the magnitude of the effect increased (Fig. 11). Incipient kinking cannot therefore be associated with reversible hysteresis in single crystals, consistent with the observations of residual stresses in polycrystals in Section 3.1.1. However, if the TiC is acting as an elastic element in the two-bar model, increasing its volume fraction will increase the amount of material available to drive reverse flow in the Ti_3SiC_2 and hence increase the work done during reversible hysteresis, although there must be limits to this.

Transmission electron microscopy (TEM) of cross-sections through the indents in Ti_3SiC_2 showed clear kink-like features, numbered 1, 2 and 3 in Fig. 12a. No such features were evident in the multilayer film (Fig. 12b), where the layers were curved, even though the work dissipated was greater. This shows that the reversible hysteresis does not
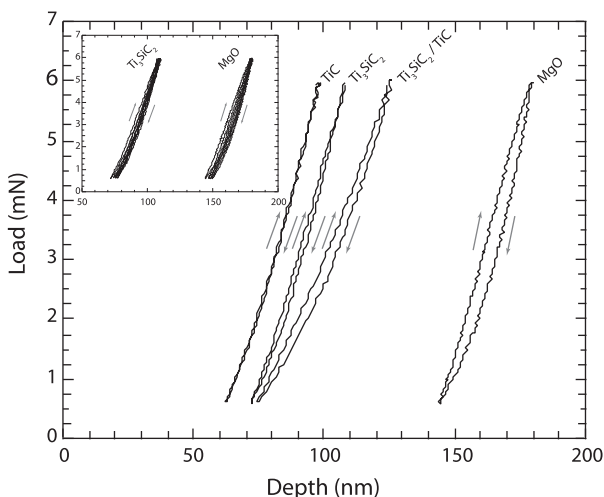
require the formation of sharp changes in curvature, as in the kink band, but can also occur where flow is more homogeneous. This raises the question of how these walls form. In Fig. 12a, there are three dislocation walls on one side of the indent, consistent with previous observations [17]. For these to have formed by kinking, as visualized by Frank and Stroh [14], two kink bands are required to have grown, with the neighbouring walls merging to form the single feature labelled 2 in Fig. 12a (enlarged in Fig. 12c). Note that the observed changes of crystal lattice curvature at features 1, 2 and 3 in Fig. 12a require that the dislocations in the merging walls have the same sign [18].

Detailed studies of what are commonly termed kink bands in the geological literature have been made in mica [49]. It was found that the kink boundaries were not sharp and have complex structures, suggesting their formation is different from that in Ref. [14]. However, it is the way in which the kink is formed that gives rise to the attractive forces between the two dislocation walls and enables reversible hysteresis.

An alternative possibility is that these features are simply dislocation walls, formed by line defects being able to move easily on the basal plane, thus allowing them to reduce their energy by aligning themselves with others on adjacent basal planes [50,51], as commonly observed in metals [52], including Zn [53] and other materials such as NaCl [54]. The formation of dislocations into walls has also been observed in the MAX phase Ti_2AlN [55]. The resulting dislocation walls would give rise to the sharp changes in crystal orientation that are a feature of deformation in these materials. Furthermore, the idea of straightforward slip occurring would also be consistent with the more diffuse slip pattern seen in multilayer structures (Fig. 12b). The movement of these walls might also account for the large, reversible changes in the volume of materials contributing to the (200) and (107) reflections observed in the in situ synchrotron diffraction study, as shown in Figs. 8 and 10.

3.2.2. Indentation in another plastically anisotropic material, MgO

To investigate the idea that reversible hysteresis is caused by the build-up of elastic strains due to plastic anisotropy, rather than kinking, some MgO crystals were indented. MgO slips most easily on the $\{1\,1\,0\}\langle 1\,\bar{1}\,0\rangle$ slip system [56]. However, this gives only two independent slip systems. Slip can also occur on the $\langle 1\,1\,0\rangle$ system, which has a critical resolved shear stress $\sim$40 times greater than the $\{1\,1\,0\}\langle 1\,\bar{1}\,0\rangle$ slip system at room temperature. Therefore, substantial elastic strains capable of driving reverse flow would be developed around the indenter, until slip is activated on the $\{0\,0\,1\}\langle 1\,1\,0\rangle$ slip system.

MgO is a very different type of material to the layered structures that have been considered so far. The bonding is ionic, and the two soft $\{1\,1\,0\}$ slip planes intersect one another in MgO, whereas the basal planes in a hexagonal material are parallel. This would make the reversible
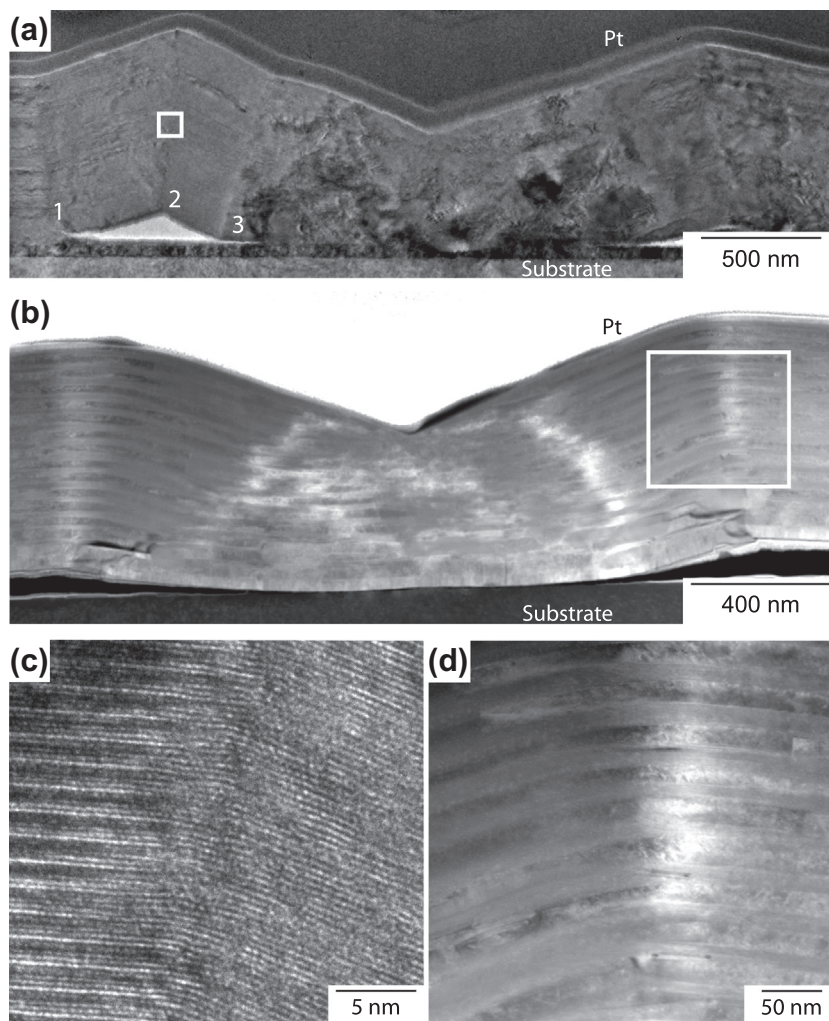

Fig. 11. The load/unloading curves obtained by nanoindentation experiments of TiC (1 1 1), Ti_3SiC_2 TiC/Ti_3SiC_2 MgO (0 0 1). The inset shows the hysteresis over four cycles for the multilayer and MgO.

Fig. 12. TEM micrograph showing a cross-section through a 50 mN indentation in (a) Ti₃SiC₂ (0 0 0 1), (b) Ti₃SiC₂/TiC multilayer, (c) the region in the square in (a), and (d) the region in the square in (b).

movement of dislocations in MgO more difficult than in the MAX phases, as there is an increased possibility of dislocation entanglement. It is only the presence of plastic anisotropy that is similar. Furthermore, MgO, being cubic, has neither a high c/a ratio nor a low value of c_{44} (155 GPa), considered to be required for reversible hysteresis. It would therefore appear to be a good test of the ideas here.

There have been many studies of indentation in cubic MgO [57–61], showing that deformation occurs by dislocation motion, with no evidence of kinking. However, kink-like features have been observed in compressed polycrystals [62] and in single crystals compressed in the hard ⟨1 1 1⟩ direction [63], where the Schmid factor on the soft {1 1 0} planes is zero.

Cyclic indentation of these MgO crystals showed reversible hysteresis (Fig. 11). This confirms that a high c/a ratio or a low value of c_{44} are not required for reversible hysteresis [3]. Furthermore, no kink-like features were observed by TEM either in the plastic zone under a larger indentation or the diffraction pattern, which showed streaking, suggesting a rather diffuse change of orientation in different parts of the crystal, consistent with dislocation flow, as opposed to the well-defined reflections arising from rotated parts of the crystal that might be expected from sharp transitions as would occur by kinking or twinning.

There must also be a component of the reversible strain associated with the elastic relaxation of dislocations in pile-ups [3]. Recently, some very elegant experiments have been carried out to measure such effects [64,65]. Locks or obstacles would normally develop during indentation, so that if relaxation of pile-ups was the predominant component of any reversible strain, reversible hysteresis would be a very common effect. However, as reversible hysteresis is not generally observed, it would seem that such relaxation is not a significant effect.

In summary, it is suggested that the effect of reversible hysteresis in single-crystal indentation may arise in any material that has sufficient plastic anisotropy that there are insufficient soft slip systems to accommodate the deformation around the indentation. The role of this anisotropy is to enable the development of elastic strains that drive reverse plastic flow.

4. Conclusions

It has been shown, in polycrystalline Ti_3SiC_2, that reversible hysteresis was only observed after the first loading cycle, during which residual elastic lattice strains developed and remained approximately constant with further cycling, inconsistent with the ideas of incipient, or unstable, kink bands.

In situ synchrotron X-ray measurements during compression testing showed that residual elastic lattice strains tend to be compressive in grains unfavourably oriented for slip, and tensile in grains where they are more favourably oriented for slip, consistent with the ideas of flow in a polycrystalline aggregate. On loading, stresses, or lattice strains, build up in these hard grains and drive reverse flow in the soft grains on unloading.

Simulations of flow in a polycrystals correctly predict the macroscopic residual strain and the reversible hysteresis effect, provided the yield stress on the basal plane is sufficiently low. The simulations also predict the magnitude of the work dissipated and its observed dependence on the maximum stress and require only the yield stress and elastic constants. However, some features of the loading and unloading diffraction data are not yet understood and further studies are needed to understand these effects.

In indentation, it is suggested that the reversible hysteresis is associated with the need for multiple slip systems to accommodate the indenter. Where the number of slip systems is limited, dislocation flow will give rise to the development of elastic strains, capable of driving reversible hysteresis. This is supported by a greater amount of work being dissipated reversibly in Ti_3SiC_2/TiC multilayer films than in Ti_3SiC_2 films, even though the TiC did not show reversible hysteresis and the Young's modulus of the TiC was greater than that of Ti_3SiC_2. Furthermore, slip was observed to be more homogeneous in the multilayer and not associated with the sharp changes in crystal orientation normally observed. These observations are not consistent with the idea that the hysteresis is associated with incipient, or unstable, kink bands. It is suggested the increase in work dissipated is due to the increase in the fraction of elastic material driving reverse flow.

It is suggested instead that the structures observed in the thin-film materials and sharp changes in crystal orientation were formed, not by kink formation, but by the easy glide of dislocations to give a low-energy configuration, consistent with observations elsewhere in Ti_2AlN. Furthermore, it avoids the need to force together dislocation walls with Burgers vectors of the same sign.

It is therefore concluded that the role of plastic anisotropy in reversible hysteresis is not to favour the nucleation of unstable, or incipient, kink bands, but rather to enable the development of elastic strains in the body that can drive reverse flow. Such an approach provides an explanation of reversible hysteresis, within the existing framework of crystal plasticity in polycrystals and in indentation, that is consistent with experimental observations, in particular giving quantitative agreement with the work dissipated during a reversible cycle and its dependence on the maximum applied stress.

References

[1] Barsoum MW, Zhen T, Kalidindi SR, Radovic M, Murugaiah A. Nat Mater 2003;2:107.
[2] Barsoum M, Murugaiah A, Kalidindi S, Zhen T. Phys Rev Lett 2004;92:1.
[3] Barsoum M, Zhen T, Zhou A, Basu S, Kalidindi S. Phys Rev B 2005;71:3.
[4] Kalidindi SR, Zhen T, Barsoum MW. Mater Sci Eng A Struct Mater 2006;418:95.
[5] Murugaiah A, Barsoum MW, Kalidindi SR, Zhen T. J Mater Res 2011;19:1139.
[6] Basu S, Barsoum MW. J Mater Res 2011;22:2470.
[7] Basu S, Barsoum MW, Kalidindi SR. J Appl Phys 2006;99:063501.
[8] Basu S, Barsoum MW, Williams AD, Moustakas TD. J Appl Phys 2007;101:083522.
[9] Basu S, Elshrief OA, Coward R, Anasori B, Barsoum MW. J Mater Res 2011;27:53.
[10] Basu S, Zhou A, Barsoum MW. J Struct Geol 2009;31:791.
[11] Basu S, Zhou A, Barsoum MW. J Mater Res 2011;23:1334.
[12] Orowan E. Nature 1942;149:643.
[13] Hess JB, Barrett CS. Trans Metall Soc AIME 1949;185:599.
[14] Frank FC, Stroh AN. Proc Phys Soc Lond B 1952;65:811.
[15] Barsoum MW, Farber L, El-Raghy T. Metall Mater Trans A 1999;30:1727.
[16] Barsoum MW, El-Raghy T. Metall Mater Trans A 1999;30:363.
[17] Molina-Aldareguia JM, Emmerlich J, Palmquist J-P, Jansson U, Hultmann L. Scripta Mater 2003;49:155.
[18] Bei G-P, Guitton A, Joulain A, Brunet V, Dubois S, Thilly L, et al. Philos Mag 2013:1.
[19] Farber L, Barsoum MW, Zavaliangos A, El-Raghy T. J Am Ceram Soc 1998;81:1677.
[20] Hutchinson JW. Proc Math Phys Eng Sci 1970;319:247.
[21] Turner PA, Tomé CN. Acta Metall Mater 1994;42:4143.
[22] Dye D, Stone HJ, Reed RC. Curr Opin Solid State Mater 2001;5:31.
[23] Jones NG, Dye D. Intermetallics 2011;19:1348.
[24] Jones NG, Ward-Close CM, Brown PM, Dye D. Scripta Mater 2010;63:85.
[25] Wilhelmsson O, Eklund P, Giuliani F, Högberg H, Hultman L, Jansson U. Appl Phys Lett 2007;91:123124.
[26] Hammersley AP, Svensson SO, Thompson A. Nucl Instrum Methods Phys Res A 1994;346:312.
[27] Korsunsky AM, Wells KE, Withers PJ. Scripta Mater 1998;39:1705.
[28] Eshelby JD. Proc Math Phys Eng Sci 1957;241:376.
[29] Eshelby JD. Proc Math Phys Eng Sci 1959;252:561.
[30] Daymond MR, Bourke MAM, Von Dreele RB. J Appl Phys 1999;85:739.
[31] Atkinson JD, Brown LM, Stobbs WM. Philos Mag 1974;30:1247.

[32] Noyen IC, Cohen JB. Residual stress: measurement by diffraction and interpretation. New York, NY: Springer Verlag; 1986.
[33] Yu R, Zhang XF, He LL, Ye HQ. J Mater Res 2011;20:1180.
[34] Emmerlich J, Högberg H, Sasvári S, Persson POA, Hultman L, Palmquist J-P, et al. J Appl Phys 2004;96:4817.
[35] El-Raghy T, Zavaliangos A, Barsoum MW, Kalidindi SR. J Am Ceram Soc 2005;80:513.
[36] Zhang ZF, Sun ZM, Zhang H, Hashimoto H. Adv Eng Mater 2004;6:980.
[37] Kooi BJ, Poppen RJ, Carvalho NJM, De Hosson JTM, Barsoum MW. Acta Mater 2003;51:2859.
[38] Gilman JJ. Cleavage, ductility and tenacity in crystals. In: Averbach BL, Felbeck DK, Hahn GT, Thomas DA, editors. Fracture. Boston, MA: Technical Press of MIT; 1959. p. 193.
[39] Lloyd SJ, Molina-Aldareguia JM, Clegg WJ. Philos Mag A 2002;82:1963.
[40] Lee SY, Kim YS, Ustundag E, Tomé C, Clausen B. Cy-SCM (EPSC), version 1.0 alpha; 2009.
[41] Taylor GI. J I Met 1938;62:307.
[42] Barsoum MW. Prog Solid State Ch 2000;28:201.
[43] Jones NG, Raghunathan SL, Dye D. Metall Mater Trans A 2010;41A:912.
[44] Bouvier S, Needleman A. Model Simul Mater Sci 2006;14:1105.
[45] Buchs R, Basu S, Elshrief OA, Coward R, Barsoum MW. J Appl Phys 2009;105:093540.
[46] Barsoum MW, Murugaiah A, Kalidindi SR, Zhen T, Gogotsi Y. Carbon 2004;42:1435.
[47] Tromas C, Villechaise P, Gauthier-Brunet V, Dubois S. Philos Mag 2011;91:1265.
[48] Hannink RHJ, Murray MJ. J Mater Sci 1974;9:223.
[49] Bell IA, Wilson CJL, McLaren AC, Etheridge MA. Tectonophysics 1986;127:49.
[50] Cahn RW. J I Met 1949;76:121.
[51] Cottrell AH. Prog Met Phys 1949;1:77.
[52] Mughrabi H. Acta Metall 1983;31:1367.
[53] Sinha PP, Beck PA. J Appl Phys 1961;32:1222.
[54] Barber DJ, Wenk H-R, Hirth G, Kohlstedt DL. Dislocations in solids: the 30th anniversary, vol. 16; 2009. p. 171.
[55] Guitton A, Joulain A, Thilly L, Tromas C. Philos Mag 2012;92:4536.
[56] Haasen P. Mater Sci Tech Ser 1985;1:1013.
[57] Khan MY, Brown LM, Chaudhri MM. J Phys D Appl Phys 1992;25:A257.
[58] Keh AS. J Appl Phys 1960;31:1538.
[59] Yoo KC, Rosemeier RG, Elban WL, Armstrong RW. J Mater Sci Lett 1984;3:560.
[60] Atkins AG, Tabor D. J Am Ceram Soc 1967;50:195.
[61] Boyarskaya YS, Zhitaru RP, Grabko DZ, Rahvalov VA. J Mater Sci 1998;33:281.
[62] Paterson MS, Weaver CW. J Am Ceram Soc 1970;53:463.
[63] Weaver CW. Philos Mag 1967;15:177.
[64] Montagne A, Audurier V, Tromas C. Acta Mater 2013;61:4778.
[65] Gaillard Y, Tromas C, Woirgard J. Acta Mater 2006;54:1409.